Dynamic Monte Carlo Simulations to Model FRET and Photobleaching in Systems with Multiple Donor–Acceptor Interactions

ARTICLE *in* THE JOURNAL OF PHYSICAL CHEMISTRY B · JUNE 2002

Impact Factor: 3.3 · DOI: 10.1021/jp014549b · Source: OAI

4 AUTHORS, INCLUDING:

Patrick Frederix
Nanosurf AG
45 PUBLICATIONS **992** CITATIONS
SEE PROFILE

H.c. Gerritsen
Utrecht University
196 PUBLICATIONS **3,873** CITATIONS
SEE PROFILE

Dynamic Monte Carlo Simulations to Model FRET and Photobleaching in Systems with Multiple Donor−Acceptor Interactions

Patrick L. T. M. Frederix[†,‡] and Evert L. de Beer*

Department of Medical Physiology, UMC Utrecht, Stratenum, P.O. Box 85060, 3508 AB Utrecht, The Netherlands

Wendie Hamelink

Department of Physiology, AMC, University of Amsterdam, P.O. Box 22660, 1100 DD Amsterdam, Amsterdam, The Netherlands

Hans C. Gerritsen

Department of Molecular Biophysics, Debye Institute, Utrecht University, P.O. Box 80000, 3508 TA Utrecht, The Netherlands

Received: December 18, 2001; In Final Form: April 29, 2002

Monte Carlo simulations were employed to model FRET in systems that included interactions between multiple donors and acceptors and photobleaching. Simulations revealed that pixel-to-pixel variations in microscopy experiments can be due both to variations in the probe distribution and to photon noise, depending on the intensity and probes per detection pixel. The Monte Carlo simulations were used to describe fluorescence experiments on (single) actin filaments using a conventional fluorescence microscope. The filaments were labeled with TRITC at phalloidin and Cy5-maleimide at cys374 and the donor−acceptor distances were taken from literature. The images show a large pixel-to-pixel variation in the fluorescence intensity and suffer from photobleaching. In experiments, the main source of noise was the probe distribution. The acceptor suffered from rapid photobleaching, which resulted in an increase of the donor intensity in time and hampers the straightforward determination of the energy transfer efficiency. The photobleaching of both the donor and the acceptor have been included in the simulations, enabling accurate modeling of the time course of the fluorescence intensities of both donor and acceptor and the energy transfer efficiency.

Introduction

Förster Resonance Energy Transfer (FRET) is a sensitive method for the study of distance between two (fluorescently) labeled sites on a nanometer scale, because it exhibits an inverse sixth-power dependence on the distance between the labels (see, for example, refs 1−3). The FRET efficiency is commonly determined from the decrease in the donor fluorescence intensity or lifetime.

In systems where multiple donors and acceptors interact, like actin filaments, the interpretation of the FRET measurements is not straightforward. In actin filaments, the distances between the monomers are comparable to typical Förster distances, and energy transfer occurs from one donor to several acceptors in the filament.

In the case of multiple acceptors per donor the energy transfer efficiency is commonly calculated statistically using the expectation value of a binomial distribution of probes in the system.[4−7] The expectation value of such a "statistical method" is the average value based on an infinitely large number of probes. In microscopy experiments on, for example, actin filaments, the number of donor probes per detector pixel (or even per actin filament) is small and the statistical method is less suitable.

Alternatively, Monte Carlo simulations (MCSs) can be used to determine the energy transfer efficiencies, without the constraint of a large number of probes.[8,9] Furthermore, MCSs can be applied to systems with arbitrary probe distributions (including the binomial distribution). This makes MCSs better suited for the study of the influence of statistical variations in the donor and acceptor densities on the FRET efficiency in microscopy experiments. In addition to spatial heterogeneities, temporal changes may occur in microscopy experiments due to photobleaching of the donor and acceptor probes. These variations are difficult to implement in the statistical method, because photobleaching of donor and acceptor and the energy transfer are mutually dependent.[10,11] An important consequence of photobleaching is that the probe distribution changes in time, e.g., in case of the actin filament the probe distribution will deviate from the binomial one when photobleaching occurs. It has been shown previously that Monte Carlo methods can provide solutions for complex rate equations.[12,13]

In this paper a MCS algorithm is presented that describes microscopy experiments on double-labeled actin filaments. The actin filaments contain a limited number of probes per detected pixel that exhibit multiple donor−acceptor interactions. Furthermore photobleaching of both donor and acceptor occurs and mutual influence exists between FRET and photobleaching. The distances between the label sites were extracted from the structure as published by Lorenz et al.[14] (further referred to as Lorenz-structure). The simulations are used to describe experi-

* Author to whom correspondence should be addressed. Tel.: +31-30-2538905. Fax: +31-30-2539036. E-mail: e.l.debeer@med.uu.nl.
[†] Also department of Molecular Biophysics Utrecht.
[‡] Current address: M. E. Müller Institute, Biocenter, University of Basel, Switzerland.

10.1021/jp014549b CCC: $22.00
Published on Web 06/08/2002

mental data, using the donor−acceptor couple tetramethylrhodamine and Cy5 at phalloidin and Cys374, respectively (R_0 = 6.5 nm). Furthermore, the MCSs are used to test the usefulness of a simple fit function through the intensity profiles.

It is beyond the scope of this study to obtain new structural information on the actin filament. Only the movement of the acceptors in the radial direction, perpendicular to the filament axis, slightly influences the (average) energy transfer efficiency (data not shown). Translations of the acceptor sites parallel to the filament axis and rotations around the filament axis had even less influence on the energy transfer efficiency (data not shown). Using a probe combination with a shorter Förster distance gives a higher sensitivity for structural changes. This is in agreement with other observations.[4,6] Instead, this study aims to show how the MCSs can be used to describe general occurring phenomena in fluorescence microscopy, like FRET involving interactions of multiple donors and acceptors, and photobleaching.

Materials and Methods

Sample Preparation. The sample preparation and construction of microscope samples with actin filaments was based on the "in vitro motility assay" and were described previously by Hamelink et al..[15] Briefly, myosin subfragment Heavy Mero-Myosin (HMM, prepared with Chymotrypsin, Sigma) was immobilized on a glass slide. Next, phalloidin-stabilized, labeled actin filaments were added to form rigor complexes with the HMM. The actin filaments were either labeled with tetramethylrhodamine-isothiocyanate (TRITC, at phalloidin, Sigma), with Cy5-maleimide (Cy5, at cys374) or double-labeled with both TRITC and Cy5. The TRITC and Cy5 in the double-labeled filaments served as donor and acceptor in the FRET experiments.

The preparation of Cy5-maleimide from commercial Cy5 succinimidyl ester (Amersham Pharmacia Biotech) was described in detail by Gruber et al.[16] Cy5-maleimide was covalently attached to cys374 of the actin using a slightly modified procedure described by Trayer and Trayer.[17] Buffers were exchanged in a PD10 column (Amersham Pharmacia Biotech) and excess of buffer was removed with a centrifugal filter device (CENTRIKON YM-10, Millipore). The acceptor label density was 16 ± 1%, as derived from the Cy5-absorbance at 649 nm (ϵ = 250 000 M^{-1} cm^{-1}) and the protein concentration that was determined using the Bradford protein assay. The acceptor-only labeled filaments were stabilized with unlabeled phalloidin (Sigma).

The fluorescence quantum yields of TRITC and Cy5 were estimated to be 0.9 and 0.28, respectively. The latter value is a lower limit (technical data: Amersham Pharmacia Biotech). The Förster distance, R_0, was calculated from the donor emission spectrum and acceptor absorption spectrum, assuming an orientation factor $\kappa^2 = 2/3$ [3] and amounted to $R_0 = 6.5$ nm. An oxygen scavenger system based on the recipe by Kishino and Yanagida[18] was added to the buffer solutions shortly before use (3 mg/mL glucose, 21 units/mL glucose oxidase, and 300 units/mL catalase, Sigma).

Experimental Setup. The FRET measurements were carried out on a homemade epi-fluorescence microscope. Light from an argon−krypton laser (λ = 531 nm, 2060−10SA, Spectra Physics) was guided to the setup using a monomode fiber. A 575 nm dichroic mirror (DM575, Nikon) was used to separate the excitation and emission light. The excitation light emerging from the fiber was focused below the actual image plane of the microscope to illuminate the whole detection area.[19]

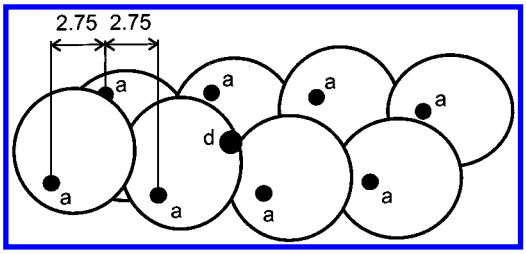

Figure 1. Schematic projection of the donor−acceptor configuration in the actin filament, showing the eight closest acceptor label-sites (*a*) at cys374 to a donor label-site (*d*) at phalloidin. The axial displacement between acceptor sites in adjacent monomers is included in nanometers.

The imaging experiments were carried out with a 40× oil immersion objective (PlanApo 1.3 NA, Nikon) and the excitation intensity at the image plane was approximately 10 W/cm^2.

The fluorescence emission was collected by the same microscope objective. After passing the first dichroic mirror the fluorescence emission was split by a second dichroic mirror that reflected light at wavelengths shorter than 660 nm and transmitted light at the longer wavelengths (Q660LP, Chroma). Two band-pass filters (HQ600/50 and HQ710/70, Chroma, for TRITC and Cy5, respectively) and an additional long-pass filter in the Cy5 emission path (BA590, Nikon) were used to suppress cross talk between the two detection channels and block scattered excitation light. Series of 8 images were recorded with a 10 s exposure time per image.

The two detection channels (TRITC and Cy5) were projected on two separate 256 × 100 pixel areas of a single CCD detector. A Peltier-cooled, slow-scan CCD camera was used for detection (Princeton Instruments, NTE/CCD-1340, 1340 × 100 pixels chip size, 16 bit ST133 controller, operated at 100 kHz ADC with readout noise 3.5e^-, Roper Scientific). The pixel size amounted to 20 × 20 μm^2. The optical system between the objective and the detector magnified the fluorescence image by a factor of 2. Consequently, the total magnification amounted to 80 times and the detector pixel size corresponded to 0.25 × 0.25μm^2 in the image plane.

Actin Structure. In actin filaments the donor and acceptor label sites are different (at phalloidin and cys374, respectively). The distances between the donor and acceptor label sites were calculated using the coordinates of the cys374 sulfide and the probe binding site of phalloidin in F-actin, as published by Lorenz et al.[14] Figure 1 gives a projection of eight successive monomers in an actin filament, showing the eight closest acceptor label-sites to a donor label-site. The distances from the donor site to its eight closest acceptor sites are 2.94, 3.50, 4.63, 5.05, 7.24, 7.95, 9.56, and 10.16 nm. When the F-actin is considered as a single (left-handed) helix, each monomer is shifted by 2.75 nm along the filament axis.[14,20] This yields 364 and 91 monomers per micrometer and pixel length, respectively.

FRET Model. In the used model the probes are described by a simple two-state model: they were either in the ground state, or in the first excited singlet state. Furthermore, in the presence of multiple acceptors, the acceptor dipoles are assumed not to interfere with each other and the interaction of a donor with the individual acceptors is considered to be independent.[4−7] Under these assumptions, the transfer rates k_{Ei} from the donor to each acceptor are pairwise additive and each can be written as if the other acceptors were absent:

$$k_{E_i} = (k_F + k_{NF}) \times \left(\frac{R_0}{R_i}\right)^6 \qquad (1)$$

with k_F and k_{NF} the fluorescent and nonfluorescent de-excitation rates, respectively, of the donor probe. R_0 is the Förster distance and R_i the distance from the donor to the ith acceptor. Fast orientation diffusion of the probe dipole moments is assumed (i.e., an orientation factor of $\kappa^2 = 2/3$),[3] and R_0 is considered identical for every donor−acceptor combination. The transfer efficiency E_i to a particular acceptor equals the ratio of the transfer rate to the acceptor and the total de-excitation rate:

$$E_i = \frac{k_{E_i}}{k_F + k_{NF} + \sum_j k_{Ej}} = \frac{(R_0/R_i)^6}{1 + \sum_j (R_0/R_j)^6} \quad (2)$$

and total energy transfer from the donor becomes

$$E_{tot} = \sum_i E_i = \frac{1}{1 + (\sum_i R_0/R_i)^{-1}} \quad (3)$$

Similar to the single donor−acceptor situation, the enhanced de-excitation rate of the donor reduces its fluorescence quantum yield, $Q_{da} = k_F/(k_F + k_{NF} + \sum_i k_{E_i})$ and hence the donor fluorescence intensity F_{da} is quenched compared to the intensity in the absence of acceptors F_d (as is the fluorescence lifetime). The change in intensity of a donor can be used to quantify the energy transfer:[3]

$$E_{avg} = 1 - \frac{F_{da}}{F_d} \quad (4)$$

Photobleaching. Photobleaching of a probe can be considered to be an irreversible de-excitation process that comes in addition to the reversible ones.[10,11] Instead of returning to the ground state the probe undergoes an irreversible reaction and is assumed to become optically inactive (i.e., nonabsorbing and nonemitting). The probability of photobleaching of a probe equals the ratio of the photobleaching rate (k_{pb}) and the total de-excitation rate ($\sum k_i$)[10] and is assumed to be independent of the excitation path: Both direct excitation by photon absorption and indirect excitation through FRET yield the same photobleaching probability.[11] In general, the photobleaching rate is much smaller than the sum of the other rates, so that $\sum k_i \approx k_F + k_{NF} + \sum k_{E_i}$. FRET influences the photobleaching of both donor and acceptor. The photobleaching probability of a donor probe is reduced by FRET: $P_{pb,da} = k_{pb,d}/(k_F + k_{NF} + \sum_i k_{E_i}) = P_{pb,d} \times (1 - E_{tot})$,[10] whereas the photobleaching of the acceptor is enhanced by FRET, because the number of excitations is increased.[11] As a result, the changes in density of the donor and acceptor probes (that are still fluorescent) are described by a set of differential equations that is generally difficult to solve analytically. The fluorescence emission of the donor in the presence and absence of acceptors, as well as the energy transfer efficiency, are now time dependent and eq 4 should be written as $F_{da}(t) = F_d(t) \times (1 - E_{avg}(t))$. Mostly, $F_d(t)$ and $E_{avg}(t)$ cannot be obtained directly and additional assumptions have to be made. In many experiments the property of interest is the initial energy transfer efficiency at the start of the experiment, $E_{avg}(0)$.

Statistical Method. In the statistical method the average energy transfer efficiency, E_{avg}, is calculated for an infinite number of donors and acceptors in the absence of (photon) noise. The E_{avg} depends on the (average) number of acceptors per donor at excitation intensities significantly below the excitation−saturation level of the probes. When the acceptor labeling of an actin filament is unsaturated, the acceptor distribution around a donor is binomial. If the number of acceptor sites contributing to the energy transfer from a donor equals N, then 2^N different combinations of labeled and unlabeled acceptor sites are possible. All combinations are different, because the N acceptor sites are located at different distances from the donor. Consequently, the total energy transfer efficiency $E_{tot,j}$ of the combination j ($\in \{1..2^N\}$) depends on the sequence of the labeled and unlabeled sites. With label density ϵ_a, the probability p_j for combination j with m labeled and $N - m$ unlabeled acceptor sites equals $p_j = \epsilon_a{}^m \times (1 - \epsilon_a)^{N-m}$. The average energy transfer efficiency E_{avg} equals the sum of the total energy transfer of each combination weighed by the associated probability of occurrence:

$$E_{avg} = \sum_{j=1}^{2^N} E_{tot,j} \times p_j \quad (5)$$

In this paper, the statistical method is applied to study the influence of the number of acceptor sites per donor (N) on the average energy transfer.

Monte Carlo Simulations. The MCSs are based on the same eqs 1− 4 as the statistical method, but now E_{avg} is simulated using finite numbers of probes and photons instead of applying eq 5. Therefore, MCSs can be used to model systems that are realistically encountered in microscopy.

The MCS require a set of input parameters describing the sample and experiment, which include: the Förster distance of the probe couple, the fluorescence quantum yields of the probes, the intrinsic (i.e., without FRET) photobleaching probabilities of the probes, the number of and positions of the label sites in a sample, the label densities of the (two) probes, the distribution function of the probes over the available label sites, and the (average) number of excitation photons per probe. The latter sets the number of simulation cycles of the MCS. The input parameters should be as much as possible obtained from independent experiments and sources. Some of the parameters relevant for actin filament are mentioned in the "sample preparation" and "actin structure" sections. The number of monomers included in each filament-fragment, the average number of excitation photons per donor, and the photobleaching probabilities were estimated from the experiment, as will be discussed later.

Using the above input parameters and random number generators the sample (i.e., an actin filament) is "constructed" and thereafter the photon-interactions are simulated. The donor and acceptor label sites (at phalloidin and cys374, respectively) were distributed randomly and independently on filaments, using their respective label densities. This yields a variation in the number of probes per actin filament (or part of it) as encountered in an experimental situation. In other applications the sample construction requires modification, using the specific properties of this sample, e.g., label sites may be nonspecific with respect to donor or acceptor.[5]

The photon-interactions were dealt with sequentially. A schematic overview of a simulation cycle of the photon interaction is shown in the flow diagram of Figure 2. In the current MCSs direct excitation of the acceptors is neglected and consequently only the donors can be excited by the photons. The donor probe site to be hit by each of the photons was selected at random. This creates a variation in the number of excitations per donor-site and allows the study of temporal changes. Photons striking a donor site without donor were counted as a cycle, but otherwise ignored. In the presence of a

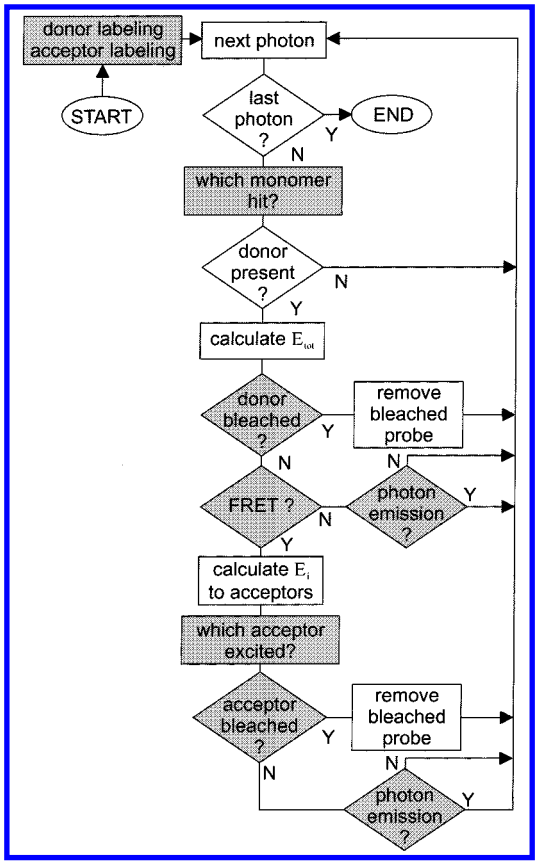

Figure 2. Flow graph of the main processes in the Monte Carlo simulations. Processes that involve random numbers are printed on a gray background.

donor the partial and total energy transfer efficiencies (E_i and E_{tot}) to the acceptors in the vicinity of the donor were calculated (eqs 2 and 3). Note, that this approach overcomes the constraint of binomial distributions of the donor and acceptor probes. To account for photobleaching, photobleaching probabilities were employed for the donors and acceptors photobleaching. Probes were removed upon photobleaching for the remaining of the simulation. The number of excitations and photon emissions were stored per donor and acceptor. The fluorescence quantum yields of the donor and acceptor were multiplied by 0.05, to account for an overall detection efficiency of the setup.

Without photobleaching the average energy transfer of a filament was calculated using eq 4. To this end, the fluorescence intensity F_{da} was calculated as the sum of the number of emitted photons by a double-labeled filament. The reference intensity F_d was the total number of emitted photons by the donors in an identical filament, but now without the acceptor labels. This method of calculating the energy transfer efficiency is comparable to that in the experiments by Bastiaens et al.[21] Here, the energy transfer efficiency was calculated from the donor fluorescence increase between two measurements, where the acceptor probes were photobleached in between.

In the presence of photobleaching this approach is not possible. As will be shown later, the photobleaching of the donor was much slower than that of the acceptor. As a result, the donor intensity increase could be approached using an exponential decay function, in which the energy transfer efficiency E_{avg} decreased exponentially and the reference intensity F_d is constant (i.e., donor photobleaching is negligible):

$$F_{da}(t) = F_d \times [1 - E_{avg,0} \times \exp\{-t/\tau_{pb,da}\}] \qquad (6)$$

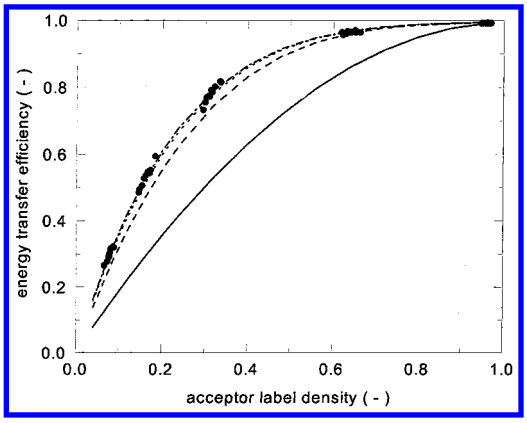

Figure 3. The energy transfer efficiency as a function of the acceptor label density at different numbers of acceptors included in the calculations. The average energy transfer is calculated from eq. 5 using $R_0 = 6.5$ nm, and including the first 2, 4, 6, or 8 (solid, dashed, dotted, and dashed−dotted lines, respectively) closest acceptor sites from a donor site in the Lorenz structure.[14]

Here, $\tau_{pb,da}$ is the time constant of the donor intensity increase in double-labeled filaments. The time t was expressed in frame numbers and was associated with the middle of the time frames. The fit could be carried out on both the experimental data and simulation data. To test the accuracy of the fit, simulation data with and without photobleaching were compared using the same (initial) probe distributions.

The simulations were carried out on a PC (DELL PRECISION 420, 800 MHz INTEL PENTIUM III processor, Dell) running WINDOWS 2000 (Microsoft). The simulation program[35] was written in IDL (version 5.3.1, Creaso) and uses the standard uniform random number generator of IDL (RANDOMU), with independent seeds for all included variables. The IDL random number generator is based on the algorithm described by Park and Miller [22] with the addition of a Bays-Durham shuffle to remove low-order serial correlations.[23] The number of excitations per donor (without photobleaching) and the variations in the number of donors and acceptors in the filament were analyzed to verify the performance of the random number generator (data not shown). The results proved that the random number generator behaved well. A typical MCS, carried out on a 10 000 monomers filament, with 4100 photons per monomer, as will be presented later, took approximately 2 h.

Results

General Controls. As a first control we verified that the MCSs yielded the 6th order distance dependence characteristic for FRET between single donors and acceptors (data not shown). Next, a calculation was carried out with the statistical method to determine the number of acceptor sites N that should be included in the MCSs in case of multiple acceptors per donor (Figure 3). Here, E_{avg} is calculated as a function of the label density ϵ_a, applying eq 5 at $R_0 = 6.5$ nm. At least the 6 closest acceptor sites should be included, in particular at lower acceptor densities. At shorter Förster distances inclusion of less acceptor sites is sufficient (data not shown). In the Monte Carlo simulations presented here, eight acceptor label sites were included per donor. This ensures that accurate E_{avg} values are found, even at the lowest label densities. In the experiments the initial acceptor label density amounted to 16% of the available sites and reduces with photobleaching. The results of several MCSs at the same Förster distance are included in the figure as open circles. Each simulation was carried out on 1000 monomers long filaments with 625 excitations per monomer

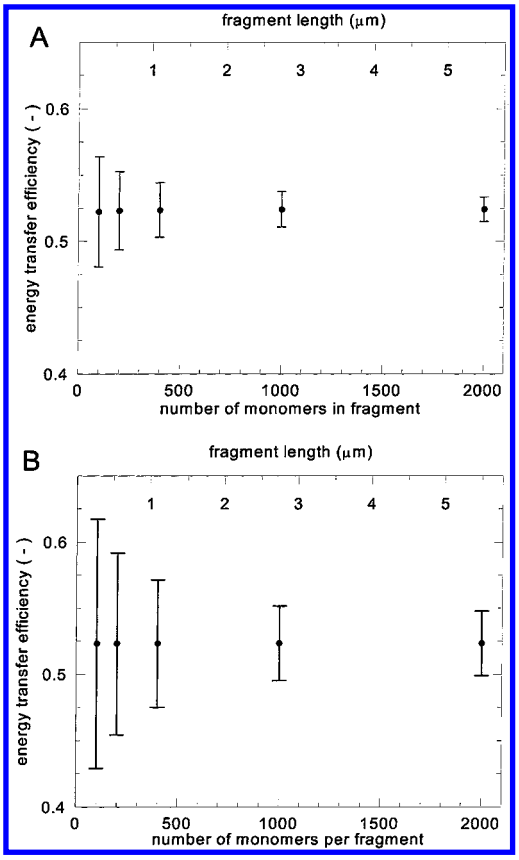

Figure 4. The standard deviation in the FRET efficiency at different fragment lengths caused by photon noise (A) and probe distribution noise (B). To obtain the influence of photon noise, the standard deviations in the FRET efficiency of 100 simulations carried out on single fragments of different lengths were calculated. Each simulation contains 100 photons per monomer on average. The average values of the standard deviations per fragment length are plotted in (A) as a function of the fragment length. In (B) the standard deviations in the FRET efficiency were calculated for multiple fragments of the same length. Here, each simulation contained 10 000 excitation photons per monomer on average to minimize the influence of photon noise. In both cases, the number of fragments per point amounts to 10 000/(fragment length).

on average. The donor label density was 90% and the acceptor label density ranged from 8 to 96%. The results of the MCSs are in close agreement with those of the statistical method. The variation in the acceptor label density of the filaments that is caused by the random labeling is clearly visible in the figure.

Photon Noise and Probe Distribution Variations. A series of simulations was carried out on filaments of different length to study the dependence of the FRET efficiency on "noise" in the donor and acceptor labeling and the influence of photon noise on differently sized fragments. The differently sized fragments (100, 200, 400, 1000, or 2000 monomers) of a 10 000 monomers long filament were analyzed independently. The number of fragments per length equals the ratio of the total number of monomers and the fragment length. To study the influence of photon noise, the average value and the standard deviation of the transfer efficiency were calculated per fragment from 100 repetitive simulations with 100 excitation photons per monomer on average. Figure 4A shows the influence of the photon noise on the standard deviation in the value of E found in the simulations at different fragment lengths. The relative standard deviation in E at 100 monomers per fragment was around 10%, and showed a decrease with the square root of the number of monomers in the fragment. Increasing the average number of excitation photons per monomer also resulted in a reduction of the photon noise by the square root of the relative increase (data not shown). The influence of the label distribution in a fragment is illustrated in Figure 4B. The average and standard deviation in the value of E of different fragments were calculated for the different fragment lengths. A large relative standard deviation of 20% was observed at 100 monomers per sub-filament that decreases at longer fragment lengths.

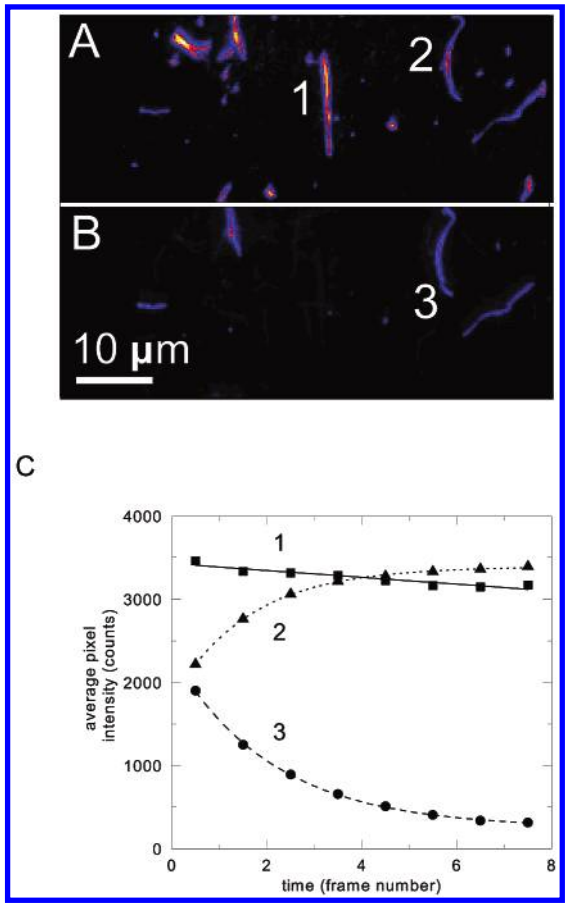

Figure 5. FRET measurement on actin filaments labeled with donor, acceptor, and donor plus acceptor. (A) Donor fluorescence image. (B) Acceptor fluorescence image. (C) The average intensity time traces of the three numbered filaments in A and B. 1: Filament labeled only with donor. 2 and 3: Donor and acceptor signals of a double-labeled filament.

FRET Experiment. We carried out fluorescence measurements on both single- and double-labeled actin filaments. In the measurements significant photobleaching was present, even though an oxygen scavenging system was applied. The acceptor (Cy5) appeared to be particularly sensitive to photobleaching. Therefore, analysis of the measured data was not possible by the statistical method. Figure 5 shows a typical fluorescence image at 531 nm excitation wavelength containing three different types of actin filaments: donor-only labeled, acceptor-only labeled, and double-labeled with both donor and acceptor. Figure 5, A and B, show the first time frames of the donor and acceptor fluorescence, respectively. The donor-only and double-labeled filaments can be easily distinguished. The filaments labeled with acceptor-only were barely visible, showing that direct acceptor excitation is negligible at 531 nm. The two images were corrected for the background. This was accomplished by subtracting the average intensity of an area in the image without any visible filaments.

The average fluorescence behavior of two different filaments in time is plotted in Figure 5C: one single-labeled with donors (1), the other double-labeled (2 and 3). The donor-only labeled

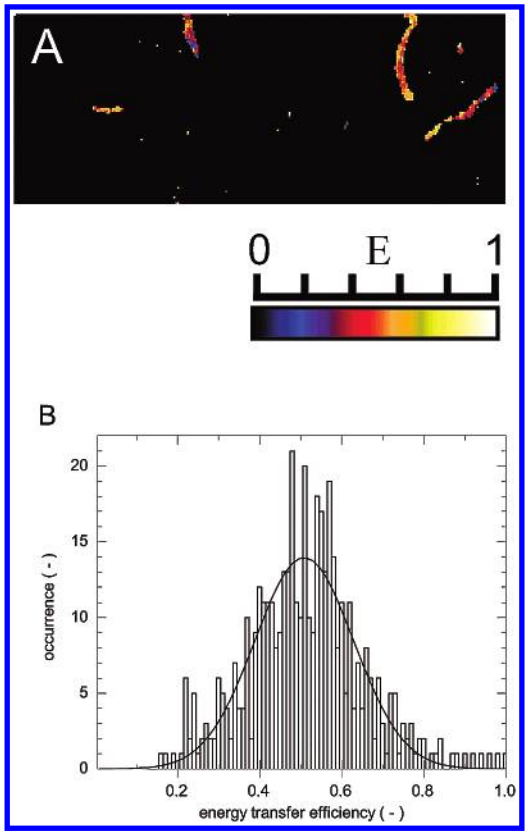

Figure 6. FRET efficiency calculated per pixel of the measurement shown in Figure 5, applying eq 6. (A) Image of the FRET efficiency per pixel, and (B) histogram of the FRET efficiencies of A. The solid line is a Gaussian fit through the data.

filament shows minor photobleaching. The acceptor intensity in the double-labeled filament decreases rapidly, while the donor intensity increases simultaneously. This is indicative for the occurrence of FRET. The intensity increase of the donor in the double-labeled filament was fitted using eq 6.

The fit was carried out per camera pixel employing a threshold to exclude pixels lacking a filament. The fit results showed large pixel-to-pixel variations in the photobleaching decay times and FRET efficiencies. The latter is shown in the image of the energy transfer efficiency and its histogram of Figure 6A and B, respectively. A Gaussian fit was employed to calculate the average value and standard deviation of the FRET efficiencies (Table 1). The photobleaching of the acceptor signal was also fitted by an exponential decay function. The photobleaching decay times of the donor-only labeled filaments were calculated from a linear fit through the data, because of the slow photobleaching. The average photobleaching decay times and FRET efficiency of the fits are presented in Table 1.

The statistical method predicts an average energy transfer efficiency of $E_{avg} = 0.523$. The results of the MCSs, with and without photobleaching are given in Table 1. The average number of photons per monomer was estimated from the experiment. It was calculated from the intensity profile of a donor-only labeled filament perpendicular to the filament direction. This yielded a total of 1.5×10^4 counts per 0.25 μm filament length (i.e., per pixel length). This corresponds with 3×10^5 emitted photons per pixel from a donor-only labeled filament per time frame. Here, we assumed a 5% overall detection efficiency of the microscope plus CCD camera. At 90% donor label density, 90% fluorescence quantum yield and 91 monomers per pixel length, this corresponds to 4.1×10^3 excitations per donor. For this reason, the (average) number of photons per monomer in the simulations was chosen at 4100.

The shown simulations were carried out on n fragments of 100 monomers long ($n = 100$). The number of monomers per fragment was chosen so that the standard deviations of the simulations and the experiment were approximately equal. As a reference, MCSs were also carried out without photobleaching. The resulting energy transfer efficiency, applying eq 4, is shown in the last column of Table 1. Because the simulation approach with photobleaching is comparatively time-consuming and a more quantitative comparison of model and experiment is desirable, a simpler fitting approach has been tested. Here, the measured and simulated donor intensity of double-labeled filaments was fitted with an exponential function (eq 6). Because we are dealing with discrete numbers of donor and acceptor probes and donor photobleaching does occur in real experiments, the exponential fitting approach requires validation. Furthermore, the photobleaching induces a deviation from the binomial distribution, which may also jeopardize this fitting approach.

To validate the fitting approach, MCSs with and without photobleaching of the probes were compared, using filaments with the same probe distributions. The average energy transfer efficiency E_{avg} in the case of photobleaching was calculated using the exponential fit. The values found for E_{avg} did not significantly differ (based on a Student's t-test, $p < 0.05$), proving the effectiveness of this fitting approach to take photobleaching into account.

Accordingly, the fit results were used as a figure of merit to compare the experimental results with the Monte Carlo simulations in a more quantitative way (see Table 1). To compare simulation data with the experimental data, the photobleaching probabilities of donor and acceptor were varied until the simulated photobleaching decay times of the donor-only labeled segments and those of the donor and acceptor signals of the double-labeled segments matched those obtained in the experiments. The match was closest at intrinsic photobleaching probabilities of 4.5×10^{-6} and 3.6×10^{-5} for the donor and acceptor, respectively. The fit results of simulations are listed in Table 1. The values of E_{avg} (at $t = 0$) were somewhat lower for the experiment (significant at $p < 0.05$, Student's t-test). For comparison, the table lists the results of MCSs that were carried out using a 10% larger acceptor photobleaching probability as well as results without donor photobleaching.

Discussion and Conclusions

General Controls. Monte Carlo simulations were employed as a tool to model FRET in double-labeled actin filaments exhibiting multiple donor−acceptor interactions. The program code revealed the typical sixth-order distance dependence for FRET between single donor and acceptor probes. Furthermore, using large numbers of monomers and photons the average energy transfer obtained by the MCSs was in close agreement with those obtained by the statistical method. This is an indication of the correctness of the program code.

Photon Noise and Probe Distribution Variations. When applying the MCSs on a limited number of actin monomers and using a limited number of photons, a considerable variation in the energy transfer efficiency per filament fragment was found without photobleaching (see Figure 4). The two main causes are the photon noise and variations in the probe distribution. In the latter, the number of acceptors had most influence (see also the simulation points in Figure 3). The precise sequence of the probes in a filament proved to be of less importance. This was investigated by repeatedly distributing a fixed number of donors

TABLE 1: The Photobleaching Time Constants and Energy Transfer Efficiencies for the Measured Data and the MCSs[a,b,c,d]

		donor-only	double-labeled		transfer efficiency	
$P_{pb,don}$	$P_{pb,acc}$	$\tau_{pb,donor}$	$\tau_{pb,donor}$	$\tau_{pb,acceptor}$	fitted	no photo bleaching
IVMA:						
N. A.	N. A.	64 ± 36	1.8 ± 1.0	2.4 ± 1.0	0.51 ± 0.10	N. A.
MCS's:						
4.5×10^{-6}	3.6×10^{-5}	62 ± 17	1.8 ± 1.0	2.6 ± 1.2	0.54 ± 0.14	0.52 ± 0.10
4.5×10^{-6}	4.0×10^{-5}	63 ± 20	1.55 ± 0.66	2.28 ± 0.86	0.54 ± 0.15	0.52 ± 0.10
0	3.6×10^{-5}	$>10^3$	2.9 ± 1.0	2.9 ± 1.1	0.56 ± 0.11	0.52 ± 0.11

[a] Photobleaching time constants, τ_{pb}, are expressed in numbers of frames.[b]The number of included pixels in the fits of the experimental data are as follow: 476 for the donor labeled filaments and 442 and 367 for the donor and acceptor signals of the double-labeled filaments. The presented values are the averages with the standard deviations of the distributions. [c] The simulation input is described in the text. [d] The statistical method yields $E_{avg} = 0.523$ using the same input (without photobleaching).

or acceptors at random positions on a filament and carrying out MCSs (data not shown). Because the number of label sites per detection unit (i.e., per camera pixel in widefield microscopy or focal volume in confocal microscopy) is generally limited in microscopy, probe noise is expected to occur more generally.

Figure 4, A and B, can be seen as the influence of pixel binning (giving a larger detection unit and hence more monomers per detection unit) on the noise level, with respect to both probe variations and photon noise. Furthermore, the MCSs can be used to estimate the required detection intensity to reduce the photon noise to a level that is much lower than the probe distribution noise. It should be noted that the spreading of the intensity over multiple detector pixels (perpendicular to the filament axis) is not incorporated in the noise analysis. An even spreading over 4 pixels would yield a relative noise increase of a factor of 2. In this case, the relative standard deviation of the photon noise becomes identical to that of the probe distribution noise at 100 photons per monomer.

Standard Deviation in the Experiments. The number of excitations per monomer was estimated to be over 4000 photons. Consequently, the experimentally found standard deviation in the FRET efficiency is ascribed to the variations in probes per pixel and not to photon noise. In general, a large standard deviation limits the usefulness of the FRET experiments. Here, the MCSs could be used to compare the standard deviations of the experiment with those found in the simulations. The comparison helped with the estimation of the number of monomers that significantly contribute to the intensity in each detector pixel. The number of monomers included in each filament-fragment (100) was close to the number of monomers per detector pixel in the microscope that was estimated to be 91. As a result of a lateral point spread of the fluorescence signal in the microscope, the fluorescence signal from one monomer spreads over more than one pixel. Similarly, the intensity collected in each pixel originates from more than the 91 monomers. However, the contribution of a specific monomer decreases with increasing distance (of the projection) of the monomer to the center of a pixel. On the basis of these arguments and the resemblance between the measurements and the simulations the use of 100 monomers long fragments appears justified.

Although the standard deviations of the donor and acceptor time constants in the double-labeled filament experiments and simulations were in close agreement, a large discrepancy was found in the standard deviation of the photobleaching decay times of the donor-only labeled filaments. Here, the standard deviation in the experimental results was significantly larger than in the simulations. The photobleaching decay time constant of the donor-only labeled filaments was much longer than the total acquisition time. This made the calculation of the decay time sensitive to variations in the background and other environmental variations.

Photobleaching. In the discussed experiment the acceptor was particularly sensitive to photobleaching. When eq 4 is applied to the donor intensity in the first and last frame of the recording, the acceptor photobleaching during the recording of the first frame would have lead to an erroneous value for E_{avg} of less than 0.4. Shortening the acquisition time can reduce this error at the expense of a higher photon noise. From the MCS-based noise analysis, it is expected that at 100 instead of 4100 excitation photons per monomer, the photon noise would be comparable to the noise from the limited number of probe molecules.

Here we have tried to obtain $E_{avg}(0)$ by incorporating the photobleaching in the analysis. To this end, the experimental intensity curves of only donor and double-labeled actin filaments were simulated using MCSs and an exponential fitting approach. The exponential decay function can be justified by the lower photobleaching of the donor compared to that of the acceptor, and the linearity of the energy transfer efficiency with the acceptor density. This can be inferred from Figure 3 where the FRET efficiency is plotted as a function of the acceptor label density. The comparison of the simulation data with and without photobleaching proved the validity of the used fitting approach.

The lower FRET efficiency of the experiment compared to the MCSs may have several causes.

Both traces of free probe in the actin stock solution and photobleaching of acceptor before the start of the measurement lead to an overestimation of the acceptor label density. To reduce photobleaching before the start of the experiment, focusing was carried out at the lowest possible excitation intensities and short acquisition times of the camera. The difference in E_{avg} may also be explained by an overestimation of the Förster distance. The discrepancy is less likely to be explained by a deviation from the Lorenz structure. It can be calculated from the Lorenz structure (applying, e.g., the statistical method) that a radial acceptor displacement of more than 0.5 nm is required to obtain a reduction of 0.03 in E.

The donor photobleaching was assumed negligible in the exponential fits. In both the simulations and the measurements of the double-labeled filaments, the time constant associated with the donor intensity increase was shorter than that of the acceptor intensity decrease. This is explained by the presence of some residual photobleaching of the donor. The MCSs without donor photobleaching yielded identical values for the two time constants (see Table 1). Although the donor photobleaching did influence the (fitted) time constants associated with the fluorescence intensity changes, the FRET efficiencies of the MCSs with and without donor photobleaching agreed reasonably well (see Table 1). Neglecting the photobleaching

was further justified by its low intrinsic photobleaching probability compared to that of the acceptor. The FRET process further reduced the photobleaching of the donor.[10] Moreover, the high donor-to-acceptor density ratio caused a higher average number of excitations per acceptor than that per donor.

The FRET efficiencies obtained by fitting the MCSs was not very sensitive to the acceptor photobleaching rate. A 10% increase in the acceptor photobleaching probability affected only the photobleaching decay times and not the fitted transfer efficiency.

Other donor−acceptor combinations, in particular, combinations with faster donor photobleaching, require a more complex approach, because donor photobleaching has to be incorporated in the fit procedure. Higher acceptor densities also require a more complex approach, because at higher acceptor densities the relation between E_{avg} and the acceptor label density is nonlinear anymore and the donor intensity can no longer be approximated by an (single) exponential function. This was confirmed by MCSs.

The fitted time courses of the donor and acceptor fluorescence intensities yielded estimated values for the different photobleaching probabilities. The acceptor was found to have a higher photobleaching probability than the donor. The two main reasons for the difference in photobleaching behavior of the donor and acceptor are: (1) the intrinsic difference in the photostability of the two probes (TRITC versus Cy5 under the same conditions), (2) probes at the phalloidin site are less prone to photobleaching than at the Cys374 site. The Cys374 is located at the exterior of the F-actin, while the phalloidin site is buried inside the F-actin and thus better shielded from the environment. This was concluded from a comparison of the photostability of actin filaments labeled with tetramethylrhodamine at phalloidin and at Cys374 (data not shown). The photobleaching probability of TRITC found here is within the range of values reported for rhodamine (10^{-5}−10^{-7}).[19,24,25] It should be noted that the found values scale with the (assumed) values of several parameters (e.g., fluorescence quantum yield and detection efficiency), which limits the accuracy of the found probabilities.

Extensions of the Simulations. The MCSs presented here did not include all possible probe interactions. The effects of such interactions on the experiments are expected to be small, as concluded from the good agreement between the experiments and the simulations. However, it is believed that the method can be easily modified or extended for other applications, where other interactions are significantly involved. It might for example be useful to include homo-FRET from donor-to-donor or acceptor-to-acceptor or backward energy transfer from acceptor to donor[26] in the MCSs. For other experiments the simple two-state model to describe the energy levels of the probes, with photobleaching from the excited state,[10,11] may be insufficient. Incorporation of the triplet state in the model enables the inclusion of more complex decay processes, in particular those related to saturation or photobleaching.[27−29]

In our model we assumed fast, rotational diffusion of the probes (i.e., $\kappa^2 = 2/3$). Based on both literature[3] and the presented experimental results, this assumption appears valid for the used probe combination in this sample. Deviations from $\kappa^2 = 2/3$ will yield different Förster distances R_i for each of the donor−acceptor combinations that can be both lower and higher. When this information is available, variation of κ^2 can be included in the MCSs through the Förster distances. On the other hand, when sufficient other information is available, it is not impossible to deduce κ^2 from the comparison of experiments with MCSs.

Another potential application for the MCSs as described here, might be the simulation of FRET between a semiconductor nanoparticle (quantum dot) and an organic dye.[30] In this case additional de-excitation paths and recombination paths are required to describe the intermittency in the quantum dot emission.[31−34] In conclusion, the Monte Carlo simulations proved to be a versatile method to model spatial and temporal fluorescence intensity fluctuations in microscopy with multiple applications in the future.

Acknowledgment. The authors thank Hermann Gruber (Institute of Biophysics, J. Kepler University, Linz, Austria) for the preparation of Cy5-maleimide and Ben Treijtel (Department of Physiology, AMC, University of Amsterdam, The Netherlands) and Dave VandenHeuvel (Department of Molecular Biophysics, Debye Institute, Utrecht University, The Netherlands) for technical support. Yehudi Levine (Computational Biophysics, Debye Institute, Utrecht University, The Netherlands) and Andries Meijerink (Condensed Materials Debye Institute, Utrecht University, The Netherlands) are gratefully acknowledged for the fruitful discussions. The Netherlands Council for Earth and Life Sciences (ALW) of The Netherlands Organization for Scientific Research (NWO) financially supported this project.

References and Notes

(1) Förster, T. *Ann. Phys.* **1948**, *2*, 55−75.
(2) Stryer, L.; Haugland, R. P. *Proc. Natl. Acad. Sci. U.S.A.* **1967**, *93*, 719−726.
(3) Dos Remedios, C. G.; Moens, P. D. J. *Resonance energy transfer*; Wiley: Sussex, 1999; Chapter 1, pp 1−64.
(4) Moens, P. D. J.; Yee, D. J.; Dos Remedios, C. G. *Biochemistry* **1994**, *33*, 13102−13108.
(5) Li, M.; Reddy, L. G.; Bennet, R.; Silva, N. D.; Jones, L. R.; Thomas, D. D. *Biophys. J.* **1999**, *76*, 2587−2599.
(6) Nyitrai, M.; Hild, G.; Lukács, J.; Bódis, E.; Somogyi, B. *J. Biol. Chem.* **2000**, *275*, 2404−2409.
(7) Xu, J.; Root, D. D. *Biophys. J.* **2000**, *79*, 1498−1510.
(8) Hisada, K.; Ito, S.; Yamamoto, M. *J. Phys. Chem. B* **1997**, *101*, 6827−6833.
(9) Meskers, S. C. J.; Hübner, J.; Oestreich, M.; Bässler, H. *J. Phys. Chem. B* **2001**, *105*, 9139−9149.
(10) Jovin, T. M.; Arndt-Jovin, D. J. *Annu. Rev. Biophys. Biophys. Chem.* **1989**, *18*, 271−308.
(11) Mekler, V. M.; Averbakh, A. Z.; Sudarikov, A. B.; Kharitonova, O. V. *J. Photochem. Photobiol. B* **1997**, *40*, 278−287.
(12) Fichthorn, K. A.; Weinberg, W. H. *J. Chem. Phys.* **1991**, *95*, 1090−1096.
(13) Binder, K. *Monte Carlo methods in statistical physics*, 2nd ed.; Springer Verlag: Berlin, 1986.
(14) Lorenz, M.; Popp, D.; Holmes, K. C. *J. Mol. Biol.* **1993**, *234*, 826−836.
(15) Hamelink, W.; Zegers, J. G.; Treijtel, B. W.; Blangé, T. *Anal. Biochem.* **1999**, *273*, 12−19.
(16) Gruber, H. J.; Kada, G.; Pragl, B.; Riener, C.; Hahn, C. D.; Harms, G. S.; Ahrer, W.; Dax, T. G.; Hohenthanner, K.; Knaus, H.-G. *Bioconjugate Chem.* **2000**, *11*, 161−166.
(17) Trayer, R. H.; Trayer, I. P. *Biochemistry* **1988**, *27*, 5718−5727.
(18) Kishino, A.; Yanagida, T. *Nature* **1988**, *334*, 74−76.
(19) Schmidt, T.; Schütz, G. J.; Baumgartner, W.; Gruber, H. J.; Schindler, H. *Proc. Natl. Acad. Sci. U.S.A.* **1996**, *93*, 2926−2929.
(20) Dos Remedios, C. G.; Moens, P. D. J. *Biochim. Biophys. Acta* **1995**, *1228*, 99−124.
(21) Bastiaens, P. I.; Majoul, I. V.; Verveer, P. J.; Soling, H. D.; Jovin, T. M. *EMBO J.* **1996**, *15*, 4246−4253.
(22) Park, S. K.; Miller, K. W. *Commun. ACM* **1988**, *31*, 1192−1201.
(23) Press: W. H.; Flannery, B. P.; Teukolsky, S. A.; Vetterling, W. T. *Numerical recipes in C*, 2nd ed.; Cambridge University Press: Cambridge, 1994.
(24) Rosenthal, I. *Opt. Commun.* **1978**, *24*, 164−166.
(25) Huston, A. L.; Reimann, C. T. *Chem. Phys.* **1991**, *149*, 401−407.
(26) Bojarski, P.; Kulak, L. *Chem. Phys.* **1997**, *220*, 323−336.
(27) Tsien, R. Y.; Waggoner, A. *Handbook of biological confocal microscopy*. 2nd ed.; Plenum Press: New York, 1995; Chapter 16.

(28) Song, L.; Hennink, E. J.; Young, I. T.; Tanke, H. J. *Biophys. J.* **1995**, *68*, 2588−2600.

(29) Song, L.; Varma, C. A.; Verhoeven, J. W.; Tanke, H. J. *Biophys. J.* **1996**, *70*, 2959−2968.

(30) Willard, D. M.; Carillo, L. L.; Jung, J.; Van Orden, A. *Nanoletters* **2001**, *1*, 469−474.

(31) Nirmal, M.; Daboussi, B. O.; Bawendi, M. G.; Macklin, J. J.; Trautman, J. K.; Harris, T. D.; Brus, L. E. *Nature* **1996**, *383*, 802−804.

(32) Efros, A. L.; Rosen, M. *Phys. Rev. Lett.* **1997**, *78*, 1110−1113.

(33) Kuno, M.; Fromm, D. P.; Hamann, H. F.; Gallagher, A.; Nesbitt, D. J. *J. Chem. Phys.* **2000**, *112*, 3117−3120.

(34) Van Sark, W. G. J. H. M.; Frederix, P. L. T. M.; Van den Heuvel, D. J.; Asselbergs, M. A. H.; Senf, I.; Gerritsen, H. C. *Single Mol.* **2000**, *1*, 291−298.

(35) The IDL program listing is available on request.